Chapter 6

Fabrication of Polyimide Porous Nanostructures for Low-k Materials

Takayuki Ishizaka and Hitoshi Kasai

Additional information is available at the end of the chapter

http://dx.doi.org/10.5772/53458

1. Introduction

The processing speeds of microchips continue to increase as integration densities increase in the semiconductor industry. When the device size is decreased, the so-called resistance–capacitance (RC) delay and the crosstalk noise between metal interconnects offset any gain in chip performance. To avoid these undesirable phenomena, lower dielectric insulating layers must be employed. In the near future, it will be need to develop dielectric materials with ultralow dielectric constants (ultralow-*k*: $k < 2.0$), and a replacement dielectric for carbon-doped silicon dioxide (SiOC) will be required [1]. In addition, high-thermal stability, good adhesion to metals and chemical stability are also important requirements for the interlayer dielectrics. Polyimides (PIs) are among the most promising candidates for use as next-generation interlayer dielectrics because of satisfying all above-mentioned requirements. Indeed, PIs have been widely employed in the fields of microelectronics applications such as substrate of flexible printed circuitry boards, insulating layers in multilevel very-large-scale integrated (VLSI) circuits and buffer coatings in electronic packages. However, the dielectric constant (k) is about 2.4~3.0 even in fluorinated PIs [2-7], which are insufficient for the requirement of ultralow-*k* materials ($k < 2.0$).

According to the Maxwell-Garnett model [8], it is well known that porous structures in PI films could substantially reduce dielectric constants, because the dielectric constant of air is unity. Therefore, many studies on porous PI films have been reported. The porous PI films have been generally prepared by pyrolysis of thermally labile polymer units in phase-separated PI composite films [9-12]. Namely, so-called nanofoams were produced in a PI film, resulting in providing a low dielectric constant ($k = 2.56$). Their pore sizes are also easily controlled by a component ratio of the copolymer. On the other hand, we have proposed the deposition of PI nanoparticles (NPs) onto a substrate as a novel alternative approach toward the preparation of low-*k* ($k < 2.5$) PI films, that is, by introducing air voids

between the PI NPs (Fig. 1a). To obtain ultralow-*k* PI films, we have focused on incorporating pores into the individual PI NPs and the subsequent assembly of multilayered films of porous PI NPs (Fig. 1b). This strategy must be a relatively simple and effective means for introducing air voids uniformly into ultralow-*k* PI films.

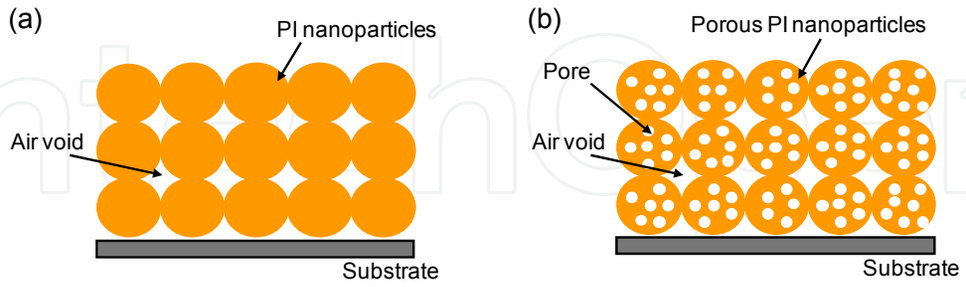

Figure 1. Schematic illustration of our strategy to reduce the dielectric constant (*k*).

In this chapter, we represent fabrication of PI NPs and morphological controlled PI NPs, *i.e.*, variously-sized NPs [13], soccer-ball-like NPs [14], cage-like microparticles [14], golf-ball-like NPs [15-17] and hollow NPs [18], using our technique, the *reprecipitation method* [19]. Furthermore, fabrication of multilayered films of porous PI NPs and their dielectric property are described [18,20].

2. Polyimide nanoparticles

Polymer fine particles are very useful for chromatographic packings; functional coatings; inks and toners; additives for foods, medicines and cosmetics; supports for catalysts; drug delivery systems; optics; and so forth. Polymer fine particles are usually manufactured during polymer synthesis from a monomer, for example, in suspension, emulsion and dispersion polymerizations. The preparations of fine particles of vinyl polymers, *e.g.* polystyrene (PS) and poly(methyl methacrylate) (PMMA), have been well-established by above-mentioned methods, and circumstantially described elsewhere. However, there are a few reports on fine particles of non-vinyl polymers including PI. Lin *et al.* [21] performed the fabrication of submicrometer PI spheres by a cooling a *N*-methyl-2-pyrrolidone (NMP) solution of PI (not PAA), which were given in high temperatures (90°C). Chai *et al.* [22] and Xiong *et al.* [23] obtained PI spheres by the dropwise addition of the precipitant (water or ethanol) into PI solutions. These methods are useful for only soluble PIs because PIs are generally insoluble in common solvents. On the other hand, precursor polymer of PI, poly(amic acid) (PAA), which is generally synthesized by polymerization of tetracarboxylic acid dianhydride and diamine, dissolves in some organic solvents such as NMP, and is easily converted into PI by the imidization treatment, namely, heat treatment or addition of cyclodehydration reagents (Fig. 2). Therefore, PI particles are often fabricated from PAA solutions or PAA particles. Nagata *et al.* [24], Asao *et al.* [25] and Basset *et al.* [26] have reported on poor-solubility PI microparticles prepared by the precipitation polymerization method, *i.e.*, the thermal imidization of PAA dissolved in NMP, which acts as a good solvent for PAA but a poor solvent for PI. Okamura *et al.* [27] precipitated uniform PAA particles of

submicron scale by the precipitation polymerization between pyromeritic acid dianhydride and 4,4'-diaminodiphenyl ether in acetone, followed by imidizing these PAA particles. Recently, a few studies on fabrication of polymeric particles composed of PI and other materials (*e.g.* PS , silica) have been also reported [28-31]. On the other hand, we have reported on the reprecipitation method, which is a simple and facile fabrication technique for polymer particles and organic nanocrystals [19,32-34]. We have successfully fabricated PI NPs via the reprecipitation method [13-18]. Furthermore, novel composite PI NPs have been also fabricated by this method [35,36].

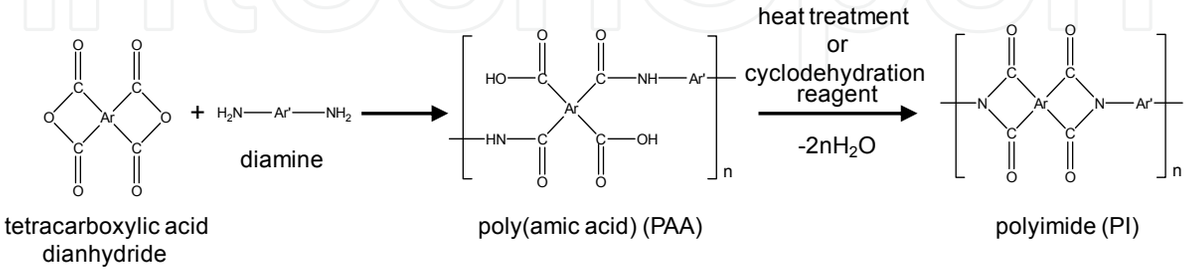

Figure 2. Synthesis route to polyimide.

2.1. Fabrication of polyimide nanoparticles via the reprecipitation method

We have successfully fabricated NPs of various PIs shown in Fig. 3. The fabrication procedure is described as follows. Because PIs are generally insoluble in common organic solvents, we used PAA solutions as starting materials for fabrication of PI NPs. Figure 4 shows the schematic representation of PI NPs via the reprecipitation method. PAA NPs were firstly fabricated by the reprecipitation method and then were converted to PI NPs through the "two-steps imidization", *i.e.* chemical imidization of PAA NPs in the dispersion medium with cyclodehydration reagent, followed by thermal imidization. In a typical experiment, a dispersion liquid of PAA NPs was obtained by injecting NMP solution of PAA (100 μl) into a vigorously stirred poor solvent (10 ml, containing 0.1 wt% of dispersing agent, Acrydic A-1381 (Dainippon ink and chemicals, Inc.)). In the present case, carbon disulfide (CS_2), cyclohexane and their mixture were used as the poor solvent. Chemical imidization of PAA NPs was performed by adding 100 μl of pyridine/acetic anhydride mixture (1:1) into the PAA NPs dispersion liquid and stirring for 2 h. After the chemical imidization, the PI NPs were centrifuged and dried *in vacuo*. Finally, PI NPs were cured at 270°C for 1 h.

PAA NPs and PI NPs obtained through the two-steps imidization were all spherical shape as shown in Fig. 5. Moreover, DLS measurement showed that the mean particle sizes and their distributions almost consisted before and after the chemical imidization [13]. These results indicate that no aggregation occurred during the imidization and we can control size of PI NPs by size-controlling PAA NPs.

A conversion to PI was estimated from IR spectra shown in Fig. 6. After the two-steps imidization (c), the absorption band around 1550 cm^{-1} (amide II: CNH vibration) and 1690

cm^{-1} (Amide I: C=O stretching vibration) disappeared, while the absorption band of imide IV (bending vibration of cyclic C=O), imide II (C-N stretching vibration), and imide I (stretching vibration of cyclic C=O) newly appeared at 720 cm^{-1}, 1380 cm^{-1} and 1720 cm^{-1}, respectively. A conversion to PI was determined by the following equation [25,37].

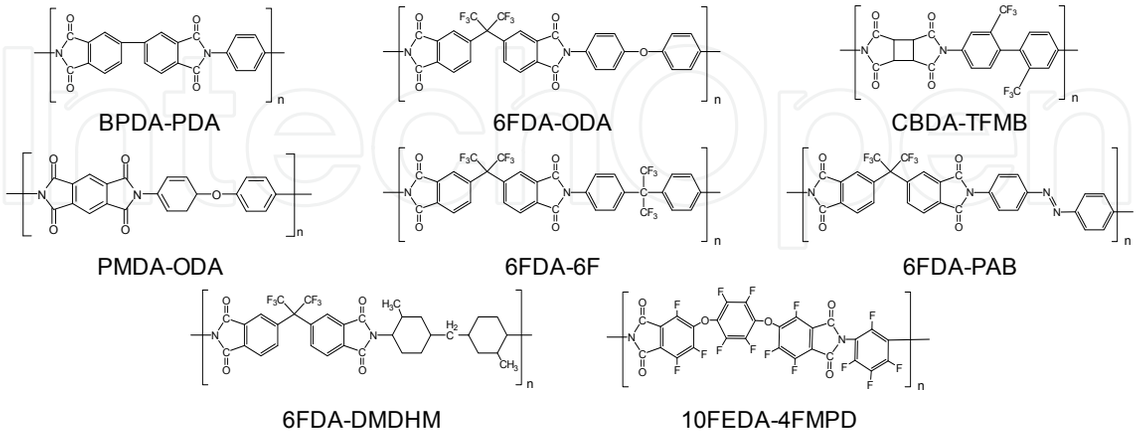

Figure 3. Structure of polyimides used in our study.

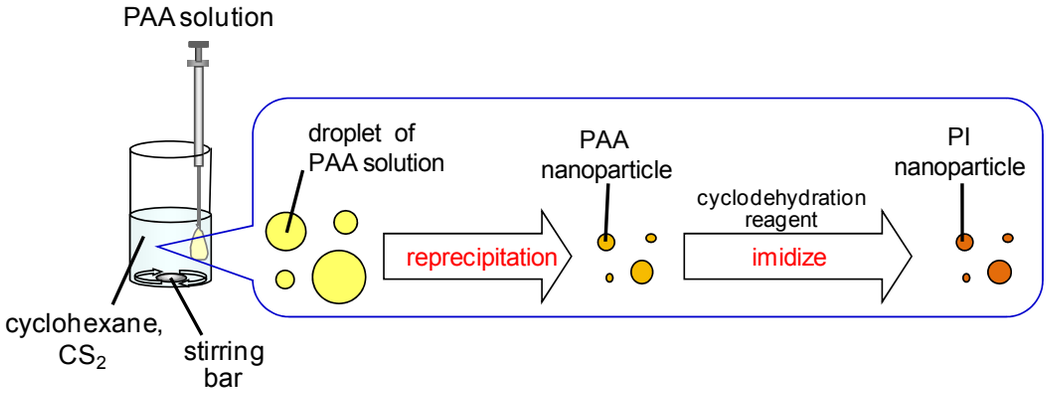

Figure 4. Schematic representation of PI nanoparticles via the reprecipitation method.

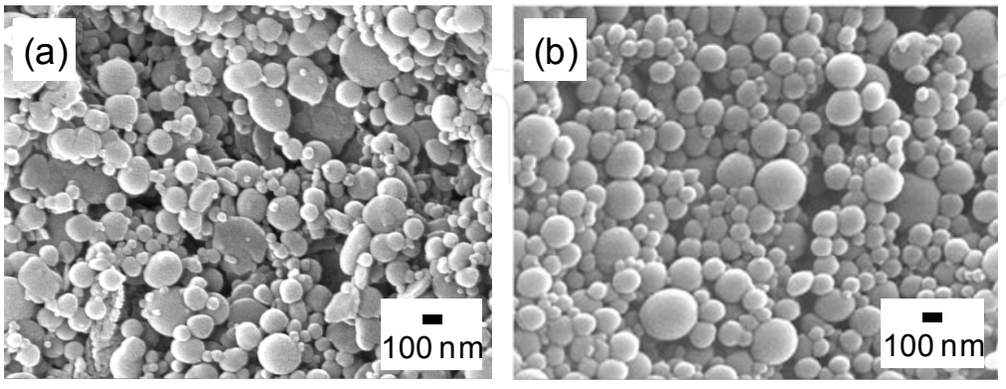

Figure 5. SEM images of 6FDA-ODA-type (a) PAA and (b) PI nanoparticles [13].

$$Conv.(\%) = \frac{\left(D_{1380\,\mathrm{cm}^{-1}} / D_{1500\,\mathrm{cm}^{-1}}\right)_{\mathrm{NPs}}}{\left(D_{1380\,\mathrm{cm}^{-1}} / D_{1500\,\mathrm{cm}^{-1}}\right)_{\mathrm{Bulk}}} \times 100, \quad (1)$$

where *D* is the optical density of each absorption bands. The absorption band at 1500 cm^{-1} (C-C stretching vibration of *p*-substituted benzene) was selected as an internal standard because its intensity remains unchanged before and after imidization. A completely-imidized sample, bulk PI, was prepared by curing a PAA cast film at 200°C for 1 h and successively at 350°C for 1 h in nitrogen atmosphere. According to the above equation, the conversion of the PI NPs was 73 % after the chemical imidization, and then the conversion of almost 100 % was found to be achieved by the subsequent curing at 270°C for 1 h. These results indicate that the imidization have been carried out quantitatively without changing their morphology.

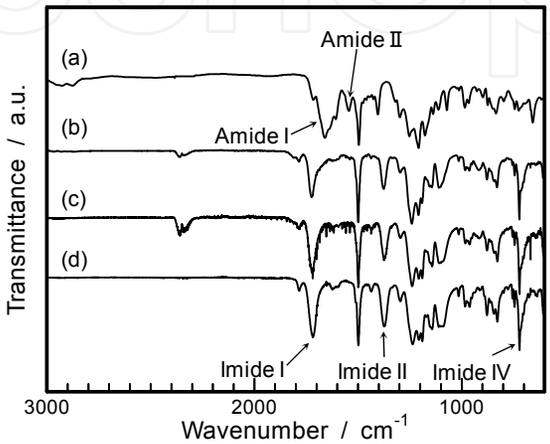

Figure 6. IR specta of (a) PAA nanoparticles, (b) nanoparticles after chemical imidization, (c) nanoparticles after two-steps imidization and (d) bulk polyimide.

2.2. Size-control of polyimide nanoparticles

As mentioned above, size-control of PI NPs will be performed by controlling size of PAA NPs. Size of PAA NPs can be decided by reprecipitation conditions such as concentration of a PAA solution (*C*), temperature of a poor solvent (T_{poor}) and species of a poor solvent (*e.g.* CS_2 and cyclohexane). Relationships between sizes of final PI NPs and reprecipitation conditions are shown in Fig. 7. As shown in Fig. 7a, a mean particle size increased with increase in *C*. This tendency is same to that in other organic compound systems previously reported [33]. To understand this phenomenon, we have to consider on the fabrication mechanism of PAA NPs using the reprecipitation method. In the reprecipitation process, first, fine droplets are dispersed in cyclohexane after injection of PAA solution. Next, NMP is removed from droplets by rapid dissolution into cyclohexane, and then PAA NPs form because PAA is insoluble in cyclohexane-rich solvent. When the concentration of the injected solution is higher, higher-concentrated droplets are produced without changing the droplet size, providing lager-sized NPs. On the other hand, a mean particle size decreased with increase in T_{poor} up to 20°C, and same size was given above 20°C (Fig. 7b). This result is explained as follows. NMP diffuses from droplets into cyclohexane slowly because of its high viscosity and poor miscibility with cyclohexane. Hence, droplets grow by agglutination between them before completion of the reprecipitation process, resulting in lager-sized particles are obtained. Under the higher temperature condition, however, the reprecipitation

process is performed in a shorter time because the diffusion rate becomes drastically higher. Thus, decrease in the particle size caused by a shorter time period for growth of droplets at higher poor solvent temperature. In addition, a mean particle size also decreased with increasing a volume rate (Φ_{CS2}) of CS_2 in a cyclohexane/CS_2 mixture (Fig. 7c). PAA NPs with a size of *ca*. 50 nm were obtained under the condition using pure CS_2 as a poor solvent. This result is explained by considering miscibility between NMP and poor solvents (cyclohexane and CS_2). A difference in solubility parameters between two kinds of solvents is often used for evaluating their miscibility, and the smaller difference means higher miscibility. The solubility parameters (δ) of NMP, CS_2, and cyclohexane were calculated by the Hansen method [38] and the values of 22.9, 20.5 and 16.8 $MPa^{1/2}$ were obtained, respectively. The differences in solubility parameters indicate that NMP/CS_2 system is higher miscibility than NMP/cyclohexane system. In the case of use of CS_2/cyclohexane mixture as a poor solvent (Fig. 7c), increase in Φ_{CS2} suggests improvement of the miscibility between NMP and poor solvents due to increase in high-miscible CS_2 for NMP. The improvement results in same effect to the temperature dependence, *i.e.*, a shorter time period for droplets growth and a decrease in a size of PAA NP. Thus, we could successfully obtain size-controlled PI NPs via the two-step imidization process. Figure 8 shows SEM images of PI NPs, which were size-controlled in the range of 20 ~ 500 nm by fabricating under various reprecipitation conditions. All PI NPs were almost spherical, free of aggregations, and quantitatively imidized.

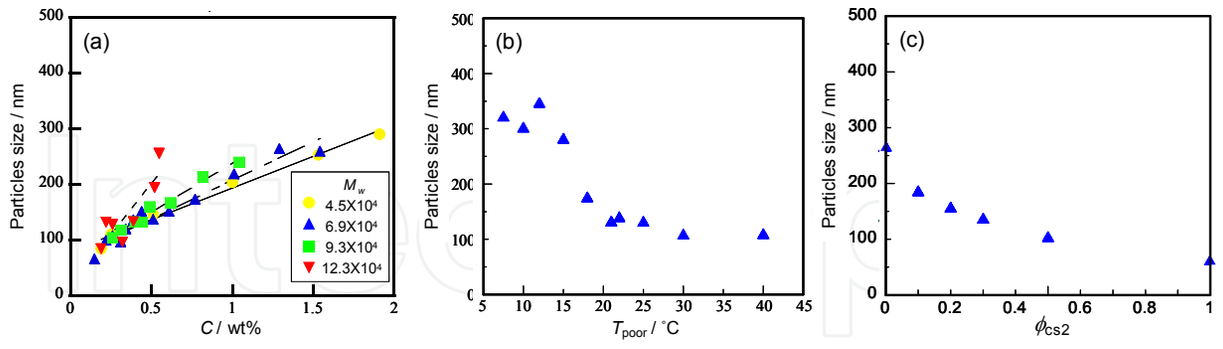

Figure 7. Relationships between size of PI nanoparticles and reprecipitation conditions [13]. Dependence of (a) concentration of PAA solution under T_{poor} = 22°C, Φ_{CS2}=0; (b) temperature of poor solvent under C=0.5 wt%, Φ_{CS2}=0, M_w=69,000; (c) volume fraction of CS_2 in poor solvent (mixture of CS_2 and cyclohexane) under C=1.5 wt% and T_{poor}=22°C, M_w=69,000.

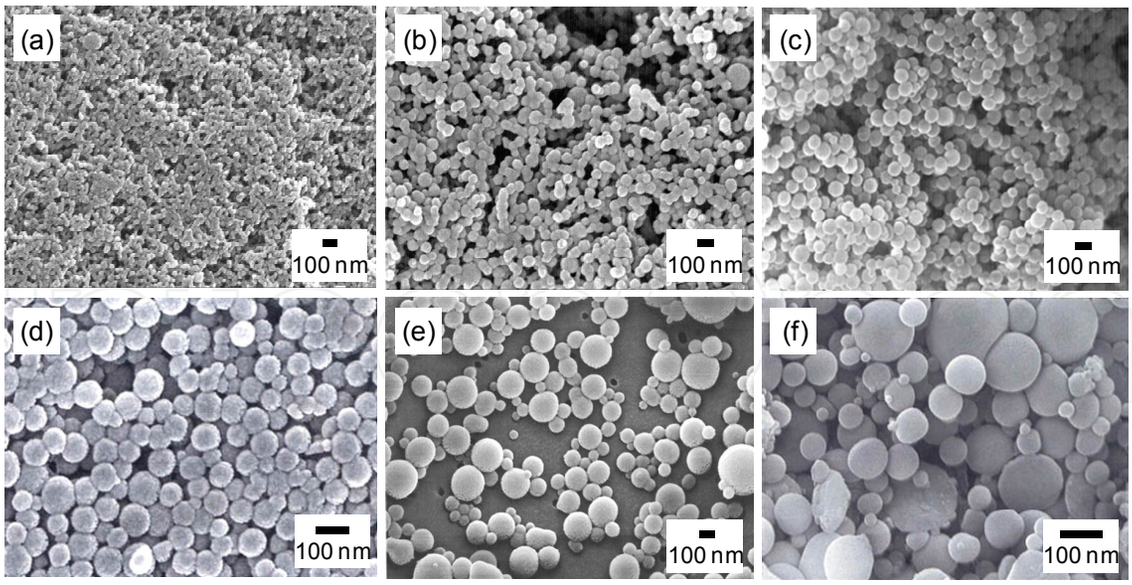

Figure 8. SEM images of 6FDA-ODA PI nanoparticles fabricated under various conditions [13]. Mean particles size: (a) 20 nm, (b) 50 nm, (c) 80 nm, (d) 100 nm, (e) 250 nm, (f) 500 nm.

3. Porous polyimide nanoparticles

Porous NPs are promising materials for low dielectric fillers, adsorbents, drug delivery systems, catalyst carriers and optics. Some studies on fabrication of porous polymer particles have been reported [39-44]. Okubo *et al.* [39] have reported fabrication of micron-sized PMMA/PS composite particles having 50~150 nm-sized dents on their surface. They achieved preparation of these particles by the seeded dispersion polymerization of styrene with PMMA seed particles in a methanol/water medium in the presence of decalin droplets. Griffiths *et al.* [40] have reported porous PS particles fabricated by the surfactant-free polymerization of styrene under the presence of water-soluble natural polymers. Kao *et al.* [41] fabricated porous poly(styrene-divinylbenzen) (PS-DVB) micoparticles by the method of multistep swelling and polymerization involving the use of polymeric porogens as follows. Monodispersed polystyrene seed particles were first prepared by the dispersion polymerization. These seeds were swollen with styrene monomer and then polymerized. Subsequently, styrene and DVB were both absorbed into the particles obtained in the previous step, and then copolymerized within the enlarged particles. In the final step, polystyrene in the particles was eluted by toluene. Unsal *et al.* [42] have also reported poly(glycidyl methacrylate-ethylene dimethacrylate) porous particles prepared by the method of swelling and seeded polymerization using PS seed particles. Koushik *et al.* [43] obtained porous deslorelin-poly(lactide-co-glycolide) microparticles by a supercritical CO_2 treatment of these sphere particles. Albrecht *et al.* [44] have reported microporous particles of poly(ether imide) prepared by a spraying/coagulation process as follows. A NMP solution of the polymer was sprayed through a hollow needle to form droplets. The droplets fell through an air gap in a water coagulation bath, which induced a phase inversion and initiated a fixation of a particle shape, and finally, the microparticles owning micoropores inside were produced. As above-

described, most of porous particles sized in the micrometer range, and few studies had been reported on porous polyimide particles [24,29]. Recently, we have successfully fabricated various types of porous polyimide NPs using the reprecipitation method [14-18].

3.1. Fabrication procedure of porous PI nanoparticles via the reprecipitation method

We have focused on incorporating pores into every single PI NPs by using microphase separation of porogen within the particles, and found that LiCl [14], poly(acrylic acid) (PA) [15,16], poly(sodium 4-styrenesulfonate) (PSS) [17], poly(methyl methacrylate) (PMMA) [18] and polyvinylpyrrolidone (PVP) [18], act as useful porogens for fabrication of porous PI NPs. The reprecipitation method was also employed in order to obtain porous PI NPs as follows. A NMP solution of PAA was prepared, and NMP solution of porogen was added subsequently. And then, PAA NPs were fabricated by injecting the polymer blend solution into cyclohexane, and two-step-imidized subsequently.

3.2. Cage-like polyimide microparticles

Interestingly, as shown in Fig. 9a and b, we could obtain some doughnut-like and hollow polyimide NPs without porogens under specific reprecipitation conditions (use of high concentrated PAA solution (e.g. 1.5 wt%) and low temperature cyclohexane (e.g. 7°C)), under which particles are mainly fabricated into the sizes larger than 1000 nm. Furthermore, we sometimes produced intriguing and uniquely shaped objects under otherwise identical conditions. For example, Figure 9c displays 300-nm-diameter polymeric soccer ball-shaped particles that exhibit both pentagonal and hexagonal facets. The line widths of the facet-frames, which are composed of polymer, were ca. 50 nm. We are unaware of any such organic and/or polymeric nanomaterials having been reported previously. We suspect that these strangely shaped NPs were fabricated through phase separation of the polymer in droplets of the solution, as indicated in Fig. 10. First, immediately after injecting the solution, the droplets were produced in cyclohexane (Fig. 10a). As N-methyl-2-pyrrolidinone (NMP) molecules in the droplets gradually dissolved in cyclohexane, the droplet size reduced. As the polymer began to precipitate at the surface of the droplet, capsule structures having sizes greater than 1 μm were formed (Fig. 10b). At this point, if all of the NMP molecules completely diffused from these capsule structures, then hollow structured nanomaterials, such as those displayed in Fig. 10c, were obtained. If, however, some of the NMP molecules remained at the surface layer, so that the polymer molecules had the flexibility to move, shrinkage of the polymer structure in Fig.10b would lead to particles having their most stable structure as that presented in Fig. 10d. Unfortunately, further research will be necessary to improve the reproducibility of our results; indeed, we successfully obtained soccer ball-shaped particles such as those in Fig. 10d less than 5% of the time. Nevertheless, we believe that the ability to prepare these new types of nanosized polymer particles should be of interest to many researchers in this field.

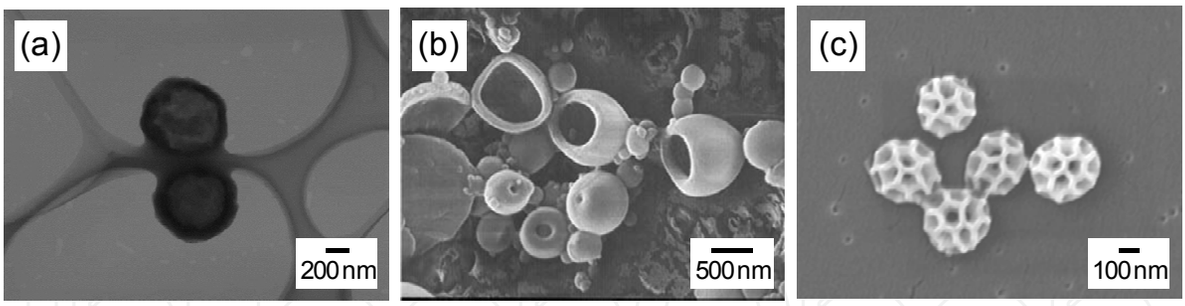

Figure 9. (a) TEM and (b), (c) SEM images of PI nanostructures fabricated by using high concentrated PAA solution and low temperature cyclohexane [14].

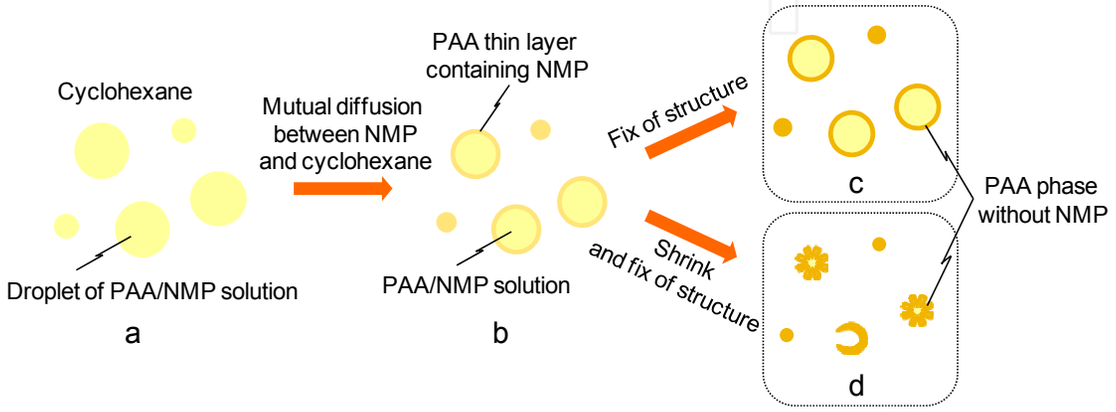

Figure 10. Schematic illustration of the process of fabricating the polyimide nanostructures.

Here, we fine-tuned the reprecipitation method to improve the reproducibility of forming porous polyimide nanostructured materials by using LiCl as a porogen. In short, a solution of poly(amic acid) (PAA) including LiCl was rapidly injected into vigorously stirred cyclohexane at room temperature. Figure 11 displays SEM images of the porous PI particles obtained after imidization and removal of the salt through washing with water. Increasing the weight ratio of LiCl to PAA in the injected solution led to an increase in the number of holes in the porous particles. The diameters of the holes on the surfaces of the particles were almost all ca. 100 nm. Figure 12 presents TEM images of the porous PI particles. We observed that spherical holes existed within the particles, which could be divided roughly into two types of porous materials. When the particle size was 700 nm or more, we observed hollow-type particles, each having a single huge hole in their center (Fig. 12a); for particle sizes below 700 nm, we observed a number of holes of almost equal size within the particles (Fig. 12b).

We have suggested a mechanism for generating these porous particles as follows. Initially, NMP droplets containing PAA and LiCl were generated in the poor solvent immediately after injection.

Next, reprecipitation of the PAA began as the NMP molecules gradually dissolved in the cyclohexane. At this stage, porous particles featuring some holes were formed in the droplets through phase separation of the polymer units. At the same time, LiCl and NMP species became concentrated within the holes. And then, NMP and LiCl eluted perfectly

from the polymer particle and into the cyclohexane. Indeed, we did not detect any LiCl in the final products. Finally, the porous PI particles were then obtained through subsequent chemical imidization.

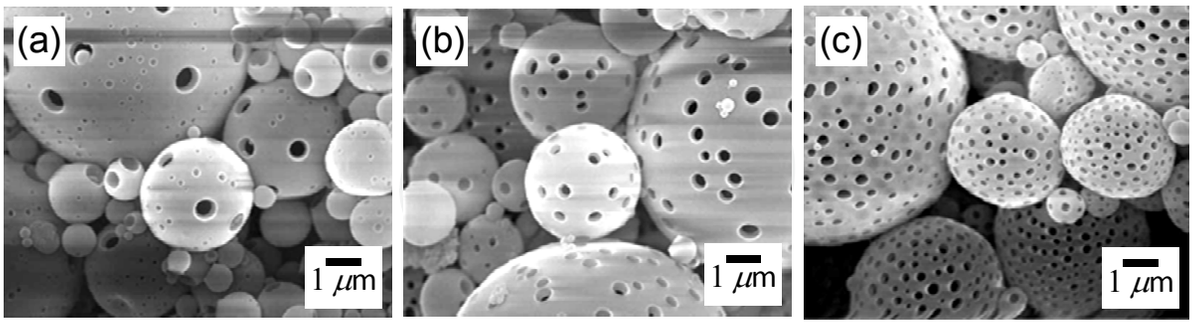

Figure 11. SEM images of porous PI particles fabricated using LiCl as a porogen [14]. Content of LiCl (relative to PAA) in the NMP solution: (a) 5, (b) 10, (c) 20 wt%.

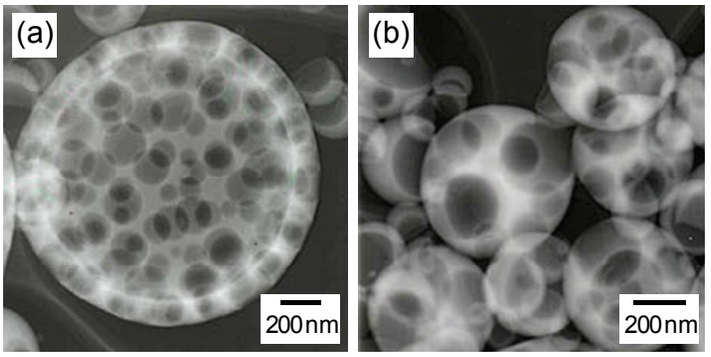

Figure 12. TEM images of the porous PI particles fabricated using LiCl as a porogen [14]. (a) Large (>700 nm) hollow-type porous particles containing a single huge hole; (b) small (<700 nm) porous particles containing multiple and equally sized holes.

3.3. Golf-ball-like polyimide nanoparticles

To fabricate porous PI NPs, the first polymer evaluated as a porogen was poly(vinyl alcohol) (PVA, M_w=500). Although both PVA and PAA (6FDA-ODA, M_w=69,000) dissolved in NMP, only some of the resulting PI NPs possessed nanopores (Fig. 13a and b). A fraction of porous PI NPs was not, however, affected by a content of PVA added. The second polymer evaluated as a porogen was poly(acrylic acid) (PA, M_w=2,000). Porous PI NPs were successfully fabricated as indicated in Fig.13c–e. The diameters of pores were in the range of 20~70 nm and the surface morphology remained almost constant when the PA content was greater than 40 wt %. Thus, PA acted as a progen for fabrication of porous PI NPs, and we have also obtained those consisted of other types of PI (10FEDA-4FMPD, BPDA-PDA and CBDA-TFMB) (Fig. 13f–h)

To consider the mechanism of formation for the porous structure, we observed SEM images of the porous PAA and/or PI NPs at each stages of their fabrication (Fig. 14). It is apparent that nanopores were already formed on the surface of the PAA NPs prior to their imidization. In addition, the surface morphology was similar before and after performing

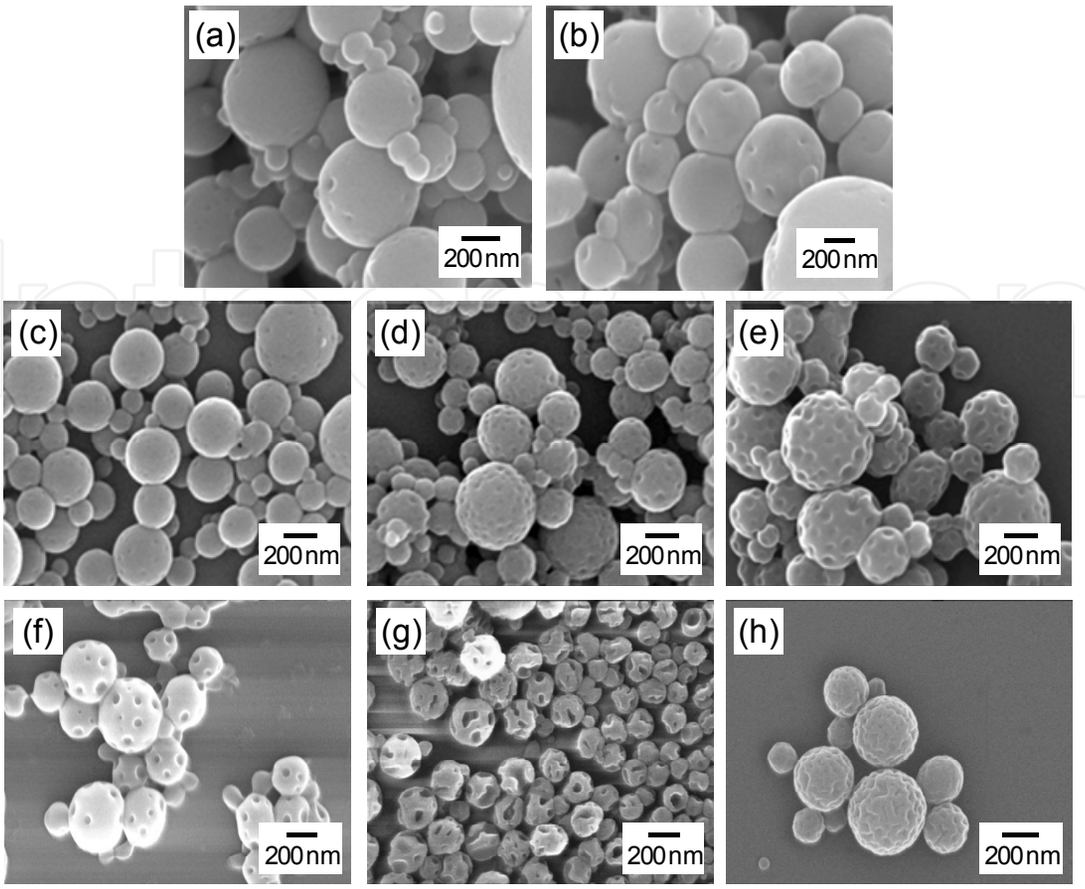

Figure 13. SEM images of porous PI nanoparticles fabricated by using various blend polymer solutions [15,16]. (a) PVA (20 wt% to PAA)/6FDA-ODA, (b) PVA (50 wt%)/6FDA-ODA, (c) PA (20 wt%)/6FDA-ODA, (d) PA (40 wt%)/6FDA-ODA, (e) PA (60 wt%)/6FDA-ODA, (f) PA (40 wt%)/10FEDA-4FMPD, (g) PA (20 wt%)/BPDA-PDA, (h) PA (40 wt%)/CBDA-TFMB.

the two-step imidization process. These findings have led us to propose a plausible mechanism of formation for the porous NPs (Fig. 15). At first, fine droplets consisting of mixture of NMP, PAA, and PA were generated in cyclohexane immediately after injection. According to the solubility parameters, cyclohexane is a much poorer solvent for PA than for PAA. As the cyclohexane and NMP diffused into one another, PAA and PA began to precipitate and microphase-separate in the surface layer of the fine droplets. At this stage, the content of cyclohexane increased gradually within each fine droplet, with NMP remaining as the main component, but with a reduced solvent power. Thus, PA-rich microdomains, which consist mainly of PA and NMP, formed within the fine droplets, because PA is more miscible with NMP. Because these internal PA-rich microdomains did not possess such a clear interface, they might have then diffused toward the surface layer. Finally, the discontinuous and isolated PA-rich microdomains that laid in the surface layer were eliminated, leading to the formation of micropores. Undoubtedly, the microphase separation giving these porous surface nanostructure is a much more complicated process than this mechanism described above; it must also depend on the molar mass of PA, the interfacial tension, the viscosity of the solvents, the mutual diffusion, and the compatibility between PAA and the porogen. With regard to this mechanism, the selection of the porogen

is very important aspect of the successful formation of the porous NPs. A suitable porogen must be compatible with PAA to some extent; a suitable choice can be determined qualitatively by comparing the difference between the solubility parameters (δ) of PAA and the porogen [45]. The solubility parameter of PA (δ_{PA}= 23.6 $MPa^{1/2}$) is closer to that of PAA ($\delta_{6FDA\text{-}ODA}$=20.8 $MPa^{1/2}$) than it is to that of PVA (δ_{PA}=30.5 $MPa^{1/2}$), which implies that PA is more compatible with PAA. Therefore, we obtained better results when using PA as the porogen.

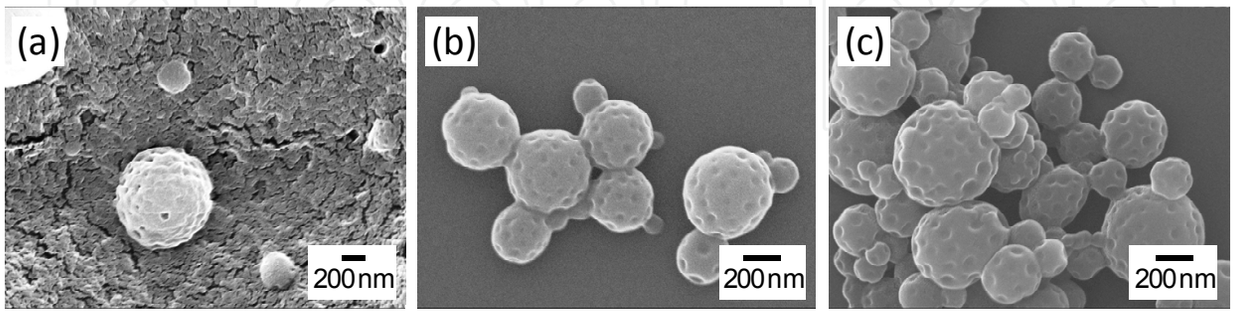

Figure 14. SEM images of porous PAA and/or PI nanoparticles at each stage of fabrication [15]. (a) immediately after injection, (b) after chemical imidization, (c) after thermal imidization.

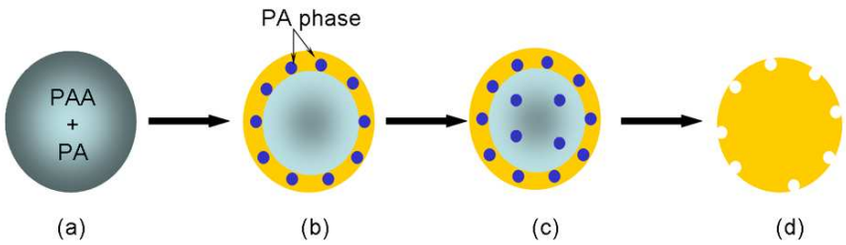

Figure 15. Schematic representation of the mechanism of formation of porous nanoparticles [15]. (a) A fine droplet of NMP, PAA, and PA formed immediately after injection; (b, c) possible intermediate states, in which the yellow regions represent zones in which NMP and cyclohexane exchange through mutual diffusion processes; (d) the resulting porous PAA NP.

It would be necessary to eliminate residual PA from the porous PI NPs if they were to be used in device applications. Figure 16 displays the results of thermogravimetric analysis (TGA) measurements. TGA curve i is that of ordinary PI NPs that lack porous structures; they decomposed thermally at a temperature above 550°C. On the other hand, PA began to decompose at ca. 200°C (TGA curve iv). The TGA curve ii is that of the chemically imidized porous PI NPs, which also decomposed gradually at ca. 200°C as a result of the removal of its residual PA and solvents. The thermally imidized porous PI NPs (TGA curve iii) yielded their 5% weight-loss temperature at 400°C; they were thermally stable up to 300°C, almost identical to the behavior of the ordinary PI NPs (TGA curve i). This result suggests that almost no PA remained within the thermally imidized porous PI NPs. Similar conclusions were drawn from the IR spectra of the various NPs. The spectrum of the thermally imidized porous PI NPs was virtually identical to that of the nonporous PI NPs. This finding suggests that PA was almost completely eliminated from the porous PI NPs during thermal imidization, consistent with the results of TGA.

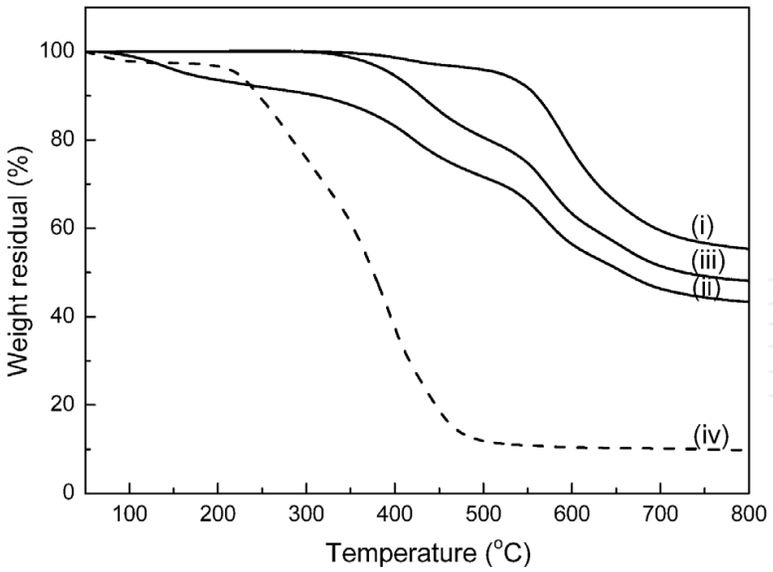

Figure 16. TGA (weight loss) curves recorded under N_2 [15]: (i) PI nanoparticles, (ii) chemically imidized porous PI nanoparticles, (iii) thermally imidized porous PI nanoparticles, (iv) PA powder. PA (40 wt %) was added to samples (ii) and (iii).

3.4. Hollow polyimide nanoparticles

By using other porogen (poly(methyl methacrylate) (PMMA) or polyvinylpyrrolidone (PVP)), hollow/multi-hollow PI NPs could be fabricated via the reprecipitation method. Figure 17 reveals that multi-hollow PI NPs were formed when we used PMMA or PVP as a porogen. Only a few small hollow cores (diameters: < 20 nm) appeared inside the PI NPs after thermal imidization when the PMMA content was 20 wt% (Fig. 17a). Upon increasing the PMMA content, larger hollow cores (diameters: ca. 100 nm), surrounded by several smaller cores, were generated; *i.e.*, the volume of the hollow structures increased accordingly (Fig. 17a–c). In contrast, we obtained only larger hollow pores ranging in a diameter from 100 to 200 nm when using PVP as a porogen (Fig. 17d, e). The number of hollow cores increased upon increasing the PVP content up to 40 wt%, but, due to high viscosity, agglomeration of the PAA NPs occurred at higher PVP contents. Clearly, the choice of a suitable porogen is an important feature affecting the generation of hollow structures. Suitable porogens can be determined qualitatively by comparing their solubility parameter with that of PAA. The solubility parameter of PAA (6FDA-ODA) ($\delta_{6FDA\text{-}ODA}$ = 20.8 $MPa^{1/2}$) is closer to that of PMMA (δ_{PMMA} = 19.7 $MPa^{1/2}$) than that of PA (δ_{PA} = 23.6 $MPa^{1/2}$), which acts as the porogen for fabrication of golf-ball-like particles (see section 3.3), indicating that PMMA is more compatible with PAA. Such a relatively high compatibility makes the PMMA phase penetrate deeper and remain within the PAA NPs, resulting in the formation of multi-hollow structures after the removal of the PMMA phase, rather than merely superficial pores. When we employed PVP (δ_{PVP} = 19.9) as an even more compatible porogen for PAA (6FDA-ODA), the PVP phases penetrated further to generate several large cores within the individual PI NPs. These findings indicate quite dramatically that the compatibility of the porogen and the PAA influences the number of hollow cores within the resulting PI NPs.

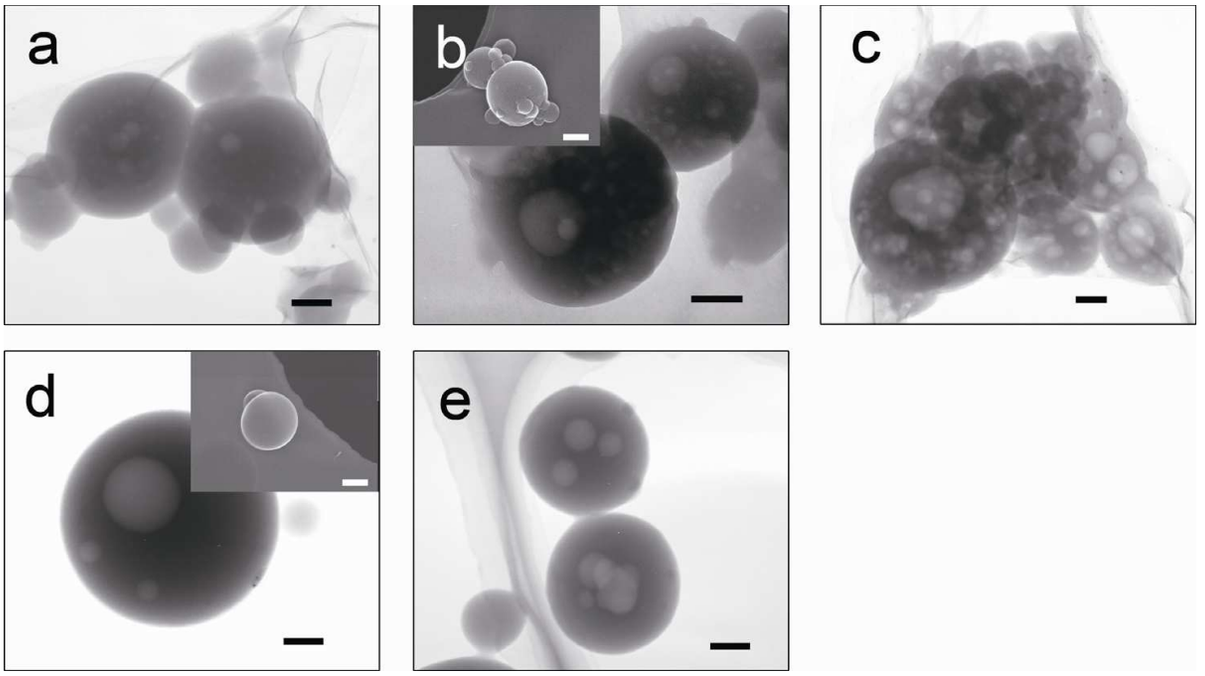

Figure 17. TEM images (scale bars: 100 nm) of multi-hollow PI(6FDA-ODA) NPs prepared using (a) PMMA 20 wt %, (b) PMMA 40 wt %, (c) PMMA 80 wt %, (d) PVP 20 wt %, and (e) PVP 40 wt % [18]. The insets display corresponding SEM images (scale bars: 200 nm).

The selection of a suitable porogen for a specific PAA allows the formation of single hollow core within each PI NP. Our approach is also applicable to other PAAs—as long as they can dissolve in the solvent. The second PI that we evaluated was PI(CBDA-TFMB) ($\delta_{\text{CBDA-TFMB}}$ = 20.0). Interestingly, the TEM images in Fig. 18 reveal only one type of hollow morphology formed—namely, a single hollow core—when using either PMMA or PVP as the porogen. Because these porogens are more compatible with PAA(CBDA-TFMB) than with PAA(6FDA-ODA), the porogen phase penetrated deeper into the center of each PI NP and integrated into a single domain, which ultimately formed the single hollow core. Moreover, the volume fraction of the hollow cores increased upon increasing the content of added PVP/PMMA. At 80 wt%, we prepared hollow PI NPs possessing core diameters in the range of 200~400 nm—the highest degree of porosity obtained in this present study.

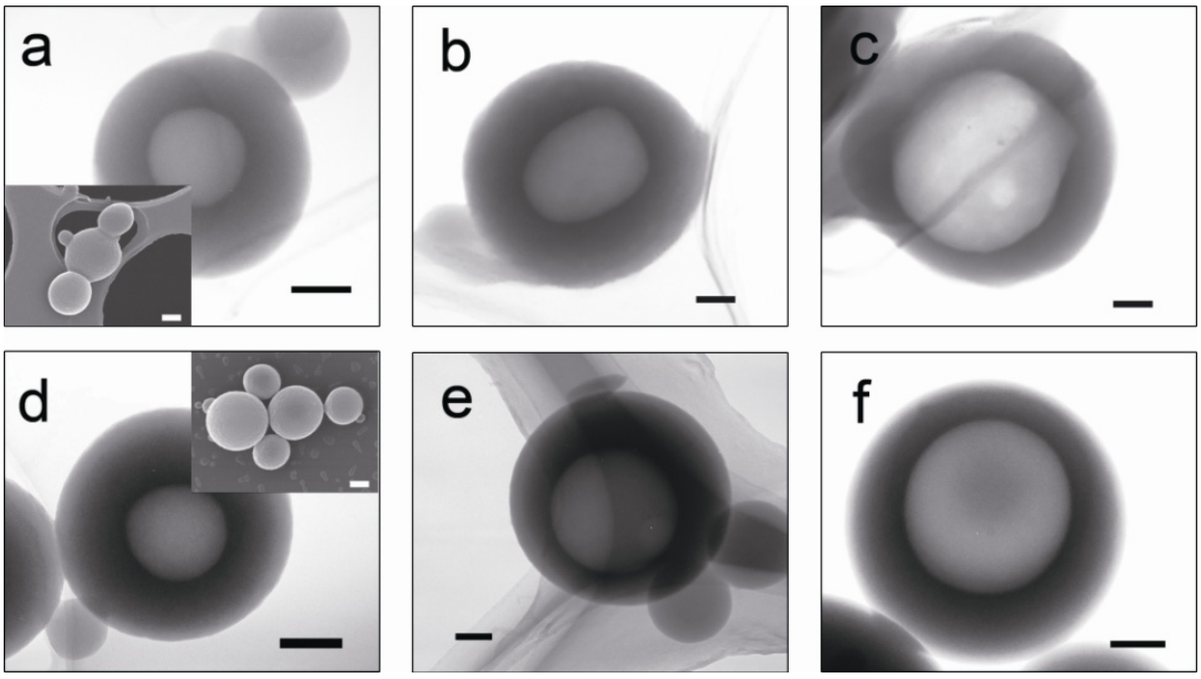

Figure 18. TEM images (scale bars: 100 nm) of hollow PI(CBDA-TFMB) NPs prepared using PMMA or PVP as the porogen at contents of (a) PMMA 20 wt %, (b) PMMA 40 wt %, (c) PMMA 80 wt %, (d) PVP 20 wt %, (e) PVP 40 wt %, and (f) PVP 80 wt % [18]. The insets display corresponding SEM images (scale bars: 200 nm).

polymer	Solubility parameter ($MPa^{1/2}$)
PAA(6FDA-ODA)	20.8
PAA(CBDA-TFMB)	20.0
poly(methyl methacrylate) (PMMA)	19.7
poly(acrylic acid) (PA)	23.6
polyvinylpyrrolidone (PVP)	19.9

Table 1. Solubility Parameters calculated using the Hoftyzer and van Krevelen method [46].

According to TGA and IR spectra of the resulting hollow PI NPs, little PVP remained within the thermally imidized hollow PI NPs, *i.e.*, the hollow PI NPs formed through thermal decomposition of the microphase-separated porogen within the composite PI/porogen NPs. This result is caused by high pyrolysis temperature of PVP (drastic weight loss from 400 to 470°C). On the other hand, PMMA was dramatically decomposed from 350 to 420°C. Therefore, no PMMA remained within the hollow PI NPs derived from the composite PI/PMMA NPs due to its lower pyrolysis temperature compared with that of PVP.

4. Low-*k* porous polyimide films

Porous PI films have been generally prepared by pyrolysis of thermally labile polymer units in phase-separated PI composite films, for example, derived from poly(propylene oxide)-,

PMMA- and poly(α-methyl-styrene)-PI block copolymer [9,10]; blend solution containing polyurethane and PAA [11]; and polyacrylamide- and PMMA-grafted PI [12]. They have achieved 10~30% decrease in a dielectric constant of polyimide films, and low-k porous films ($k \approx 2.2$) have been provided. Also, other methods, such as using water droplets and LiCl crystal as templates, and extracting a porogen polymer from composite PI film by supercritical CO_2, have been known [47-49]. On the other hand, we have obtained ultralow-k porous films by depositing porous PI NPs onto substrates [18,20].

4.1. Preparation of multilayered films of polyimide nanoparticles

We employed the electrophoretic deposition method [50] to assemble the obtained hollow PI NPs into multilayered films. The typical experiment procedure is described as follows. DC voltages were applied to indium tin oxide (ITO) electrodes immersed in a face-to-face arrangement in a suspension of PI NPs. The PI NPs, which were minus-charged in cyclohexane, were electrophoretically deposited on the anodes, and multilayered films were quickly prepared within 1 minute. The films were dried and then cured at 270 °C for 1 h to perform pyrolysis of a porogen. The electrophoretic deposition process was repeated to fill some cracks formed through coalescence of the NPs during evaporation of dispersion medium. And then, PAA solution was spin-coated onto the resulting film. After thermal imidization, a multilayer PI NPs film having a smooth surface was obtained.

Uniform films of PI NPs were easily obtained by this method as shown in Fig. 19. Furthermore, multilayered films with different thickness were prepared by changing dispersion concentration of PI NPs. As shown in Fig. 20a, film thickness increased with increase in the dispersion concentration. On the other hand, applied voltage also influenced the film thickness dramatically (Fig. 20b). Under using the dispersion liquid with solid concentration of 0.2 wt%, films became thicker as the applied voltage increased from 50 to 2000 V/cm. However, no further increase of the film thickness was observed when the applied voltage was higher than 2000 V/cm. After the electrophoretic deposition process under the applied voltage above 2000 V/cm, a transparent liquid left in sample tubes. This result indicates 100% consumption of PI NPs. Thus, the film thickness was controlled in the range of several hundred nm ~ several μm by varing dispersion concentration and applied voltage.

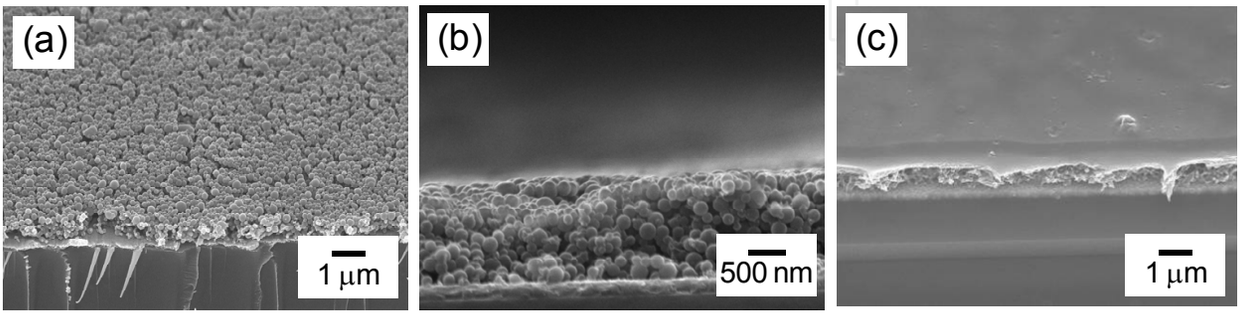

Figure 19. SEM images of multilayered films of PI nanoparticles on ITO substrates. (a) after 1st electrophoretic deposition, (b) cross section, (c) after further spin coat.

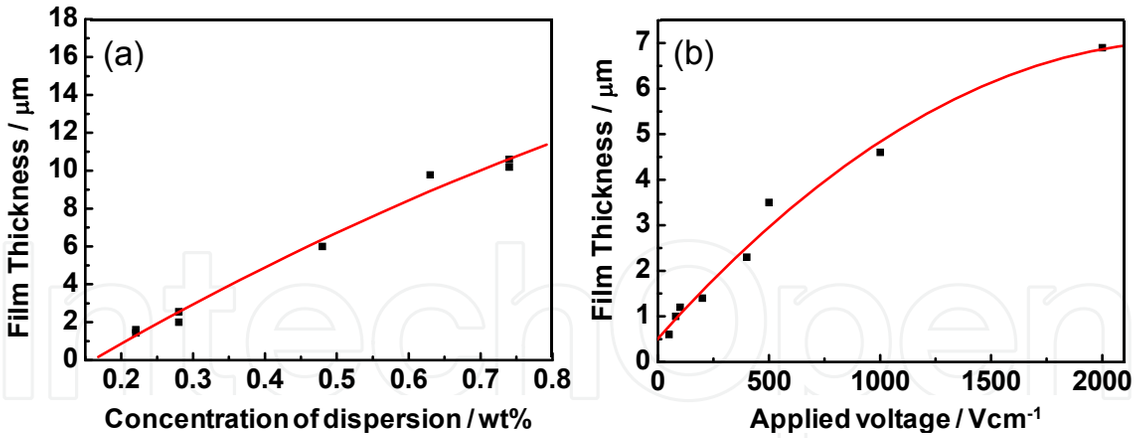

Figure 20. Dependence of (a) concentration of PI nanoparticles dispersion, (b) applied voltage, on thickness of layered film of PI nanoparlticles.

4.2. Dielectric constant of multilayered films assembled by various type of PI nanoparticles

We evaluated a dielectric constant of layered films of PI NPs prepared. Capacitance, C_p, of films was measured by a LCR meter in air and at room temperature, and a dielectric constant, k, was calculated by the equation (2).

$$k = \frac{tC_p}{\varepsilon_0 S}, \tag{2}$$

Here, C_p is a capacitance measured, t is a thickness of a film, ε_0 is the electric constant and S is an electrode area. The dielectric constants of various films, *i.e.*, cast films (non particles films), layered films of nonporous NPs and layered films of porous NPs, were summarized in Table 2. The dielectric constants of the cast films consisted of BPDA-PDA, 6FDA-ODA and CBDA-TFMB were 3.17, 2.76 and 2.52, respectively. The dielectric constants of multilayer films of nonporous PI NPs were somewhat lower, resulting from generation of air voids between NPs. The porosity of the porous films was 15~22%, calculated by using the Maxwell-Garnett model, the equation (3) [8].

$$\frac{k_{\text{porous}} - 1}{k_{\text{porous}} + 2} = \left(1 - \frac{P}{100}\right)\frac{k_{\text{solid}} - 1}{k_{\text{solid}} + 2}, \tag{3}$$

where k_{solid} is a dielectric constant of a nonporous film, and P is a porosity of a porous film. It was even lower than that of rhombohedral packing of spherical particles (porosity=26% [51]). Polydispersity of PI NPs may result in a denser packing arrangement. Moreover, the dielectric constants decreased significantly upon increasing the degree of porosity of the PI films (porosity =31~33%), *i.e.*, using hollow PI NPs instead of nonporous PI NPs. Amazingly, the dielectric constant was ca. 1.9 for the multilayer films formed from the hollow PI(CBDA-TFMB) NPs. This dielectric constant is even lower than that of a cast film of poly(tetrafluoroethylene), which has the lowest dielectric constant among polymeric

insulators. Thus, the introduction of air voids between and within the PI NPs reduced the dielectric constant significantly. In addition, the electrophoretic deposition appears to be an effective means of generating multilayer ultralow-*k* films from hollow PI NPs.

PI structures	Film types	Film thickness (μm)	Dielectric constant (*k*) @1MHz	Porosity (%)
BPDA-PDA	cast	2.14	3.17	—
	nonporous NPs	2.62	2.67	15
	golf-ball-like NPs	5.81	2.27	31
6FDA-ODA	cast	1.39	2.76	—
	nonporous NPs	3.18	2.36	17
	hollow NPs	1.90	2.00	32
CBDA-TFMB	cast	1.39	2.52	—
	nonporous NPs	4.40	2.07	22
	hollow NPs	2.50	1.87	33

Table 2. Dielectric constants and porosities of various type of PI films.

5. Conclusion

We proposed the depositing of porous polyimide nanoparticles (PI NPs) onto a substrate as the novel strategy, that is, introducing air voids within and between the PI NPs, toward the preparation of ultralow-k ($k < 2.0$) PI films. We presented fabrication of porous PI NPs and porous films, which are assembled by the porous NPs, for low-*k* materials on the basis of this strategy. In particular, Size-controlled NPs were successfully fabricated by using our technique, the *reprecipitation method,* followed by the two-step imidization. Moreover, addition of various progens, such as LiCl, poly(acrylic acid) (PA), poly(methyl methacrylate) (PMMA) and polyvinylpyrrolidone (PVP), to starting solutions of poly(amic acid) (PAA) gave cage-like, golf-ball-like, multi-hollow and hollow NPs, respectively. Also, multilayered films of porous PI NPs were successfully prepared by the electrophoretic deposition method within 1 minute. We obtained a particularly low dielectric constant (*k* = ca. 1.9) for a multilayer film assembled by one such type of hollow PI NPs. Thus, our strategy is an effective means for preparing ultralow-*k* PI films featuring unique porous structures, which are alternative candidates for use in dielectric interlayer applications.

Author details

Takayuki Ishizaka*
Research Center for Compact System,
AIST (National Institute of Advanced Industrial Science and Technology), Sendai, Japan

Hitoshi Kasai*
Institute of Multidisciplinary Research for Advanced Materials, Tohoku University, Sendai, Japan

* Corresponding Authors

Acknowledgement

Authors would like to thank Dr. M. Suzuki, Mr. H. Mitsui, Dr. G. Zhao, Prof. H. Oikawa, Prof. H. Nakanishi, Tohoku University; Prof. M. Hasegawa, Toho University and Prof. T. Furukawa, Tokyo University of Science for useful assistances and supports in this study.

6. References

[1] International Technology Roadmap for Semiconductors (ITRS), 2010 Update, Interconnect. Available: http://www.itrs.net/Links/2010ITRS/Home2010.htm. Accessed 2012 Sep 27.

[2] Anderson M R, Davis R M, Taylor C D, Parker M, Clark S, Marciu D, Miller M (2001) Thin Polyimide Films Prepared by Ionic Self-Assembly. Langmuir 17: 8380–8385.

[3] Eichstadt A E, Ward T C, Bagwell M D, Farr I V, Dunson D L, McGrath J E (2002) Synthesis and Characterization of Amorphous Partially Aliphatic Polyimide Copolymers Based on Bisphenol-A Dianhydride. Macromolecules 35: 7561–7568.

[4] Ando S, Matsuura T, Sasaki S (1992) Perfluorinated Polyimide Synthesis. Macromolecules 25: 5858–5860.

[5] Feiring A E, Auman B C, Wonchoba E R (1993) Synthesis and Properties of Fluorinated Polyimides from Novel 2,2′-bis(fluoroalkoxy)benzidines. Macromolecules 26: 2779–2784.

[6] Hasegawa M, Horiuchi M, Wada Y (2007) Polyimides Containing Trans-1,4-cyclohexane Unit (II). Low-K and Low-CTE Semi- and Wholly Cycloaliphatic Polyimides. High Perform. Polym. 19: 175–193.

[7] Hasegawa M (2001) Semi-Aromatic Polyimides with Low Dielectric Constant and Low CTE. High Perform. Polym. 13: S93–S106.

[8] Garnett J C M (1904) Colours in Metal Glasses and in Metallic Films. Philos. Trans. R. Soc. London Ser. A 203: 385-420.

[9] Hedrick J L, Miller R D, Hawker C J, Carther K R, Volksen W, Yoon D Y, Trollsås M (1998) Templating Nanoporosity in Thin-film Dielectric Insulators. Adv. Mater. 10: 1049-1053.

[10] Carter K R, DiPetro R A, Sanchez M I, Swanson S A (2001) Nanoporous Polyimides Derived from Highly Fluorinated Polyimide/Poly(propylene Oxide) Copolymers. Chem. Mater. 13: 213-221.

[11] Krishnan P S G, Cheng C Z, Cheng Y S, Cheng J W C (2003) Preparation of Nanoporous Polyimide Films from Poly(urethane-imide) by Thermal Treatment. Macromol. Mater. Eng. 288: 730-736.

[12] Wang W-C, Vora R H, Kang E-T, Neoh K-G, Ong C-K, Chen L-F (2004) Nanoporous Ultra-low-κ Films Prepared from Fluorinated Polyimide with Grafted Poly(acrylic acid) Side Chains. Adv. Mater. 16: 54-57.

[13] Suzuki M, Kasai H, Ishizaka T, Miura H, Okada S, Oikawa H, Nihira T, Fukuro H, Nakanishi H (2007) Fabrication of Size-controlled Polyimide Nanoparticles. J. Nanosci. Nanotechnol. 7: 2748-2752.

[14] Kasai H, Mitsui H, Zhao G, Ishizaka T, Suzuki M, Oikawa H, Nakanishi H (2008) Fabrication of Porous Nanoscale Polyimide Structures. Chem. Lett. 37: 1056-1057.

[15] Zhao G, Ishizaka T, Kasai H, Oikawa H, Nakanishi H (2007) Fabrication of Unique Porous Polyimide Nanoparticles Using Reprecipitation Method. Chem. Mater. 19: 1901-1905.

[16] Zhao G, Ishizaka T, Kasai H, Nakanishi H, Oikawa H (2007) Introducing Porosity into Polyimide Nanoparticles. J. Nanosci. Nanotechnol. 8: 1-5.

[17] Zhao G, Ishizaka T, Kasai H, Hasegawa M, Nakanishi H, Oikawa H (2009) Using a Polyelectrolyte to Fabricate Porous Polyimide Nanoparticles with Crater-like Pores. Polym. Adv. Technol. 20:43-47.

[18] Zhao G, Ishizaka T, Kasai H, Hasegawa M, Furukawa T, Nakanishi H, Oikawa H (2009) Ultralow-dielectric-constant Films Prepared from Hollow Polyimide Nanoparticles Possessing Controllable Core Sizes. Chem. Mater. 21: 419-424.

[19] Kasai H, Nalwa H S, Oikawa H, Okada S, Matsuda H, Minami N, Kakuta A, Ono K, Mukoh A, Naknishi H (1992) A Novel Preparation Method of Organic Microcrystals. Jpn. J. Appl. Phys. 31: L1132-L1134.

[20] Zhao G, Ishizaka T, Kasai H, Oikawa H, Nakanishi H (2007) Preparation of Multilayered Film of Polyimide Nanoparticles for Low-k Applications. Mol. Cryst. Liq. Cryst. 464: 31-38.

[21] Lin T, Stickney K W, Rogers M, Riffle J S, McGrath J E, Marand H, Yu T H, Davis R M (1993) Preparation of Sub-micron Polyimide Particles by Precipitation from Solution. Polymer 34: 772-777.

[22] Chai Z, Zheng X, Sun X (2003) Preparation of Polymer Microspheres from Solutions. J. Polym. Sci. Part B: Polym. Phys. 41: 159-165.

[23] Xiong J Y, Liu X Y, Chen S B, Chung T S (2004) Surfactant Free Fabrication of Polyimide Nanoparticles. Appl. Phys. Lett. 85: 5733-5735.

[24] Nagata Y, Ohnishi Y, Kajiyama T (1996) Highly Crystalline Polyimide Particles. Polym. J. 28: 980-985.

[25] Asao K, Ohnishi H, Morita H (2000) Preparation of Polyimide Particles by Precipitation Polymerization. Kobunshi Ronbunshu *in Japanese* 57: 271-276.

[26] Basset F, Lefrant A, Pascal T, Gallot B, Sillion B (1998) Crystalline Polyimide Particles Generated via Thermal Imidization in a Heterogeneous Medium. Polym. Adv. Technol. 9: 202-209.

[27] Okamura A, Fujimoto K, Kawaguchi H, Nishizawa H, Hirai O (1996) Preprints of 9th Polymeric Microspheres Symp.: 167 p.

[28] Omi S, Matsuda A, Imamura K, Nagai M, Ma G H (1999) Synthesis of Monodisperse Polymeric Microspheres Including Polyimide Prepolymer by Using SPG Emulsification Technique. Colloids surf. A 153: 373-381.

[29] Watanabe S, Ueno K, Murata M, Masuda Y (2006) Preparation of Polystyrene-Polyimide Particles by Dispersion Polymerization of Styrene Using Poly(amic acid) as a Stabilizer. Polym. J. 38: 471-476.

[30] Watanabe S, Ueno K, Kudoh K, Murata M, Masuda Y (2000) Preparation of Core-shell Polystyrene-polyimide Particles by Dispersion Polymerization of Styrene Using Poly(amic acid) as a Stabilizer. Macromol. Rapid Commun. 21: 1323-1326.

[31] Kim T H, Ki C D, Cho H, Chang T, Chang J Y (2005) Facile Preparation of Core-Shell Type Molecularly Imprinted Particles: Molecular Imprinting into Aromatic Polyimide Coated on Silica Spheres. Macromolecules 38, 6423-6428.

[32] Kasai H, Kamatani H, Yoshikawa Y, Okada S, Oikawa H, Watanabe A, Ito O, Nakanishi H (1997) Crystal Size Dependence of Emission from Perylene Microcrystals. Chem. Lett. 11: 1181-1182.

[33] Kasai H, Nalwa H S, Okada S, Oikawa H, Nakanishi H (2000) Fabrication and Spectroscopic Characterization of Organic Nanocrystals. In: Nalwa H S, editor. Handbook of Nanostructured Materials and Nanotechnology, San Diego:Academic Press. Chap. 8.

[34] Kasai H, Okazaki S, Hanada T, Okada S, Oikawa H, Adschiri T, Arai K, Yase K, Nakanishi H (2000) Preparation of C60 Microcrystals Using High-Temperature and High-Pressure Liquid Crystallization Method. Chem. Lett. 12: 1392-1393.

[35] Ishizaka T, Kasai H, Nakanishi H (2004) Intensity Controllable Luminescence of Eu^{3+}-doped Polyimide Nanoparticles by UV-irradiation and Thermal Treatment. Jpn. J. Appl. Phys. 43: L516-518.

[36] Ishizaka T, Kasai H, Nakanishi H (2008) Fabrication of Eu-complex/Polyimide Compostie Nanoparticles. J. Mater. Sci. 44: 166-169.

[37] Nishino T, Kotera M, Inayoshi N, Miki N, Nakamae K (2000) Residual Stress and Microstructures of Aromatic Polyimide with Different Imidization Processes. Polymer 41:6913-6918.

[38] Barton A F M (1975) Solubility Parameters. Chem. Rev. 75: 731-753.

[39] Okubo M, Takekoh R, Suzuki A (2002) Preparation of Micron-sized, Monodisperse Poly(methyl methacrylate)/Polystyrene Composite Particles Having a Large Number of Dents on Their Surfaces by Seeded Dispersion Polymerization in the Presence of Decalin. Colloid Polym. Sci. 280: 1057-1061.

[40] Griffiths P C, Wellappili C, Hemsley A R, Stephens R (2004) Ultra-porous Hollow Particles. Colloid Poly. Sci. 282: 1155-1159.

[41] Kao C-Y, Lo T-C, Lee W-C (2003) Influence of Polyvinylpyrrolidone on the Hydrophobic Properties of Partially Porous Poly(Styrene–Divinylbenzene) Particles for Biological Applications. J. Appl. Polym. Sci. 87: 1818-1824.

[42] Unsal E, Irmak T, Durusoy E, Tuncel M, Tuncel A (2006) Monodisperse Porous Polymer Particles with Polyionic Ligands for Ion Exchange Separation of Proteins. Anal. Chim. Acta 570: 240-248.

[43] Koushik K, Kompella U B (2004) Preparation of Large Porous Deslorelin-PLGA Microparticles with Reduced Residual Solvent and Cellular Uptake Using a Supercritical CO_2 Process. Pharm. Res. 21: 524-535.

[44] Albrecht W, Lützow K, Weigel T, Groth T, Schossig M, Lendlein A (2006) Development of Highly Porous Microparticles from Poly(ether imide) Prepared by a Spraying/Coagulation Process. J. Membr. Sci. 273: 106-115.

[45] Coleman M M, Serman C J, Bhagwagar D E, Painter P C (1990) A practical Guide to Polymer Miscibility. Polymer 31:1187-1203.

[46] Krevelen D W V, Nijenhuis K T (2009) Cohesive Properties and Solubility. In: Properties of Polymers, 4th Edition. Amsterdam: Elsevier Science. pp. 189-228.

[47] Yabu H, Tanaka M, Ijiro K, Shimomura M (2003) Preparation of Honeycomb-patterned Polyimide Films by Self-organization. Langmuir 19: 6297-6300.

[48] Niyogi S, Adhikari B (2002) Preparation and Characterization of a Polyimide Membrane. Eur. Polym. J. 38: 1237-1243.

[49] Mochizuki A, Fukuoka T, Kanada M, Kinjou N, Yamamoto T (2002) Development of Photosensitive Porous Polyimide with Low Dielectric Constant. J. Photopolym. Sci. Technol. 15: 159-166.

[50] Trau M, Saville D A, Aksay I A (1996) Field-induced Layering of Colloidal Crystals. Science. 272: 706-709.

[51] Graton L C, Fraser H J (1935) Systematic Packing of Spheres with Particular Reference to Porosity and Permeability. J. Geol. 43: 785.